Fractional-Order Dynamics in the Trajectory Control of Redundant Manipulators

Fernando B. M. Duarte
Dept. of Mathematics, Scholl of Technology
Polytechnic Institute of Viseu
3504-510 Viseu, Portugal
fduarte@mat.estv.ipv.pt

J. A. Tenreiro Machado
Dept. of Electrical Engineering, Institute of Engineering
Polytechnic Institute of Porto
4200-072 Porto, Portugal
jtm@dee.isep.ipp.pt

Abstract — Redundant manipulators have some advantages when compared with classical arms because they allow the trajectory optimization, both on the free space and on the presence of obstacles, and the resolution of singularities. For this type of arms the proposed kinematic control algorithms adopt generalized inverse matrices but, in general, the corresponding trajectory planning schemes show important limitations. Motivated by these problems this paper studies the chaos revealed by the pseudoinverse-based trajectory planning algorithms, using the theory of fractional calculus.

I. INTRODUCTION

The area of fractional calculus goes back to the beginning of the theory of differential calculus but its inherent complexity postponed the application of the associated concepts. In the last decade the progress in the areas of chaos and fractals revealed subtle relationships with the fractional calculus leading to an increasing interest in its development.

The area of robotics has been developed since the seventies and researchers have recognized that the addition of extra degrees of freedom (*dof*) to form a redundant arm overcomes the functional limitations of conventional non-redundant manipulators. However, the kinematic-based redundancy approaches cannot protect against unstable-chaotic joint motion and high accelerations.

Having these ideas in mind, this paper discusses a fractional calculus perspective in the study of the trajectory control of the redundant manipulators and is organized as follows. Section 2 develops the formalisms for the fractional calculus and matrix generalized inverses. Section 3 introduces the fundamental issues for the modeling of redundant manipulators. Section 4 analyses the chaotic phenomena revealed by the trajectory planning algorithms. Finally, section 5 draws the main conclusions.

II. FUNDAMENTAL ASPECTS

A. Fractional calculus

Fractional calculus is a natural extension of the classical mathematics. In fact, since the beginning of the theory of differential and integral calculus, several mathematicians investigated their ideas on the calculation of non-integer order derivatives and integrals. Nevertheless, in spite of the work that has been done the application of fractional derivatives and integrals (*FDI*s) has been scarce until recently. In the last years, the advances in the theory of chaos revealed profound relations with *FDI*s, motivating a renewed interest in this field.

The fundamentals of the fractional calculus theory and several research aspects can be addressed in references [1-4]. In what concerns the application of *FDI*s we can mention a large volume of research about viscoelasticity/damping and chaos/fractals [5-9]. However, other scientific areas are currently paying attention to the new concepts and we can refer the adoption of *FDI*s in biology, electronics, signal processing, system identification, diffusion and wave propagation, percolation, modelling and identification, chemistry and irreversibility. This work is still giving its first steps and, consequently, many aspects remain to be investigated.

Since the foundation of the differential calculus the generalization of the concept of derivative and integral to a non-integer order α has been the subject of several approaches. Due to this reason there are various alternative definitions of *FDI*s, nevertheless, from the control point of view some definitions seem more attractive, namely when thinking in a real-time calculation. The Laplace definition of a derivative of fractional order $\alpha \in C$ of the signal $x(t)$, $D^{\alpha}[x(t)]$, is a 'direct' generalization of the classical integer-order scheme yielding:

$$L\left\{D^{\alpha}\left[x(t)\right]\right\} = s^{\alpha} X(s) \tag{1}$$

In what concerns automatic control theory this means that frequency-based analysis methods have a straightforward adaptation to *FDI*s. The practical implementation of *FDI*s based on the Laplace definition adopts the frequency domain and requires an infinite number of poles and zeros obeying a recursive relationship. Nevertheless, this approach has several drawbacks. In a real approximation the finite number of poles and zeros yields a ripple in the frequency response and a limited bandwidth. Moreover, the digital conversion of the scheme requires further steps and additional approximations making difficult to analyze the final algorithm. The method is restricted to cases where a frequency response is well known and, in other circumstances, problems occur for its implementation. An alternative approach is based on the concept of fractional differential of order α. The Grünwald-Letnikov definition of $D^{\alpha}[x(t)]$ is given by:

$$D^{\alpha}\left[x(t)\right] = \lim_{h \to +0} \left[\frac{1}{\Gamma(\alpha) h^{\alpha}} \sum_{k=0}^{\left[\frac{x-a}{h}\right]} \frac{\Gamma(\alpha+k)}{\Gamma(k+1)} x(t-kh) \right] \tag{2}$$

Inspired on this definition another approximation is based on the *n*-term truncated series in the discrete-time domain, that in *z*-transform is given by:

$$Z\left\{D^{\alpha}[x(t)]\right\} \approx \left[\frac{1}{T^{\alpha}}\sum_{k=0}^{n}\frac{(-1)^{k}\,\Gamma(\alpha+1)}{k!\,\Gamma(\alpha-k+1)}z^{-k}\right]X(z) = \\ = Trunc_{n}\left(\frac{1-z^{-1}}{T}\right)^{\alpha}X(z) \tag{3}$$

An important property revealed by (2) and (3) is that while an integer-order derivative implies just a finite series, the fractional-order derivative requires an infinite number of terms. This means that integer derivatives are 'local' operators in opposition with fractional derivatives that have, implicitly, a 'memory' of all past events.

B. Generalized Inverses

This subsection addresses the generalization of the concept on matrix inversion.

For $\mathbf{A}\in\Re^{m\times n}$ and $\mathbf{X}\in\Re^{n\times m}$ the Penrose conditions:

$$\mathbf{AXA}=\mathbf{A} \tag{4}$$

$$\mathbf{XAX}=\mathbf{X} \tag{5}$$

$$(\mathbf{AX})^{T}=\mathbf{AX} \tag{6}$$

$$(\mathbf{XA})^{T}=\mathbf{XA} \tag{7}$$

Lead to the definitions:

- A *generalized inverse* of matrix **A** is a matrix $\mathbf{X}=\mathbf{A}^{-}\in\Re^{n\times m}$ satisfying condition (4);
- A *reflexive generalized inverse* of matrix **A** is a matrix $\mathbf{X}=\mathbf{A}_{r}^{-}\in\Re^{n\times m}$ satisfying conditions (4) – (5)
- A *pseudoinverse* of a matrix **A** (*Moore-Penrose inverse*) is a matrix $\mathbf{X}=\mathbf{A}^{\#}\in\Re^{n\times m}$ satisfying conditions (4)-(7).

For a matrix $\mathbf{A}\in\Re^{m\times n}$:

i) If $m < n$ and $r(\mathbf{A})=m$, then $\mathbf{AA}^{T}$ is nonsingular and

$$\mathbf{A}^{\#}=\mathbf{A}^{T}\left(\mathbf{AA}^{T}\right)^{-1} \tag{8}$$

ii) If $m > n$ and $r(\mathbf{A})=n$, then $\mathbf{A}^{T}\mathbf{A}$ is nonsingular and

$$\mathbf{A}^{\#}=\left(\mathbf{A}^{T}\mathbf{A}\right)^{-1}\mathbf{A}^{T} \tag{9}$$

iii) If $m = n$ and $r(\mathbf{A})=n$ then

$$\mathbf{A}^{\#}=(\mathbf{A})^{-1} \tag{10}$$

III. MODELLING OF REDUNDANT MANIPULATORS

This section presents, the mathematical aspects associated with the 'generalization' of classical manipulating structures by introducing extra *dof*.

A kinematically redundant manipulator is a robotic arm possessing more *dof* than those required to establish an arbitrary position and orientation of the gripper (Fig. 1). Redundant manipulators offer several potential advantages over non-redundant arms. In a workspace with obstacles, the extra degrees of freedom can be used to move around or between obstacles and, thereby, to manipulate in situations that otherwise would be inaccessible.

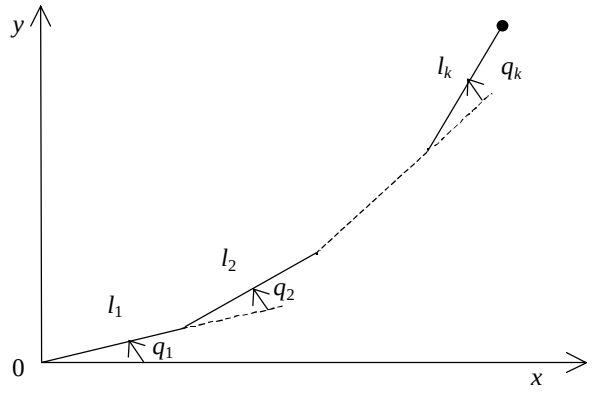

Fig. 1 A *kR* redundant planar manipulator

When a manipulator is redundant it is anticipated that the inverse kinematics admits an infinite number of solutions. This implies that, for a given location of the manipulator's gripper, it is possible to induce a self-motion of the structure without changing the location of the gripper. Therefore, redundant manipulators can be reconfigured to find better postures for an assigned set of task requirements but, on the other hand, have a more complex structure requiring sophisticated control algorithms.

We consider a manipulator with *n dof* whose joint variables are denoted by $\mathbf{q}=[q_1, q_2, ..., q_n]^{T}$ and a class of operational tasks described by *m* variables $\mathbf{x}=[x_1,x_2,..., x_m]^{T}$, $m < n$. The relation between the joint vector **q** and the manipulation vector **x** corresponds to the direct kinematics:

$$\mathbf{x}=f(\mathbf{q}) \tag{11}$$

Differentiating (9) with respect to time yields:

$$\dot{\mathbf{x}}=\mathbf{J}(\mathbf{q})\dot{\mathbf{q}} \tag{12}$$

Hence, from (10) it is possible to calculate a $\mathbf{q}(t)$ path in terms of a prescribed trajectory $\mathbf{x}(t)$. A solution in terms of the joint velocities, is sought as:

$$\dot{\mathbf{q}}=\mathbf{K}(\mathbf{q})\dot{\mathbf{x}} \tag{13}$$

where **K** is a suitable $(n\times m)$ control matrix based on the Jacobian matrix:

$$\dot{\mathbf{q}}=\mathbf{J}^{\#}(\mathbf{q})\dot{\mathbf{x}} \tag{14}$$

where $\mathbf{J}^{\#}$ is one of the generalized inverses of the **J**.

We assume that the following condition is satisfied:

$$\max\{rank\,[\mathbf{J}(\mathbf{q})]\}=m \tag{15}$$

Failing to satisfy this condition usually means that the selection of manipulation variables is redundant and the number of these variables m can be reduced. When condition (15) is satisfied, we say that the degree of redundancy of the manipulator is $n–m$. If, for some $\mathbf{q}$ we verify that:

$$rank\,[\mathbf{J}(\mathbf{q})] < m \tag{16}$$

then the manipulator is in a singular state. This state is not desirable because, in this region of the trajectory, the manipulating ability is very limited. Based on these concepts, to analyze and quantify the problem of object manipulation it was proposed [16], the expression $\mu = [det(\mathbf{J}\mathbf{J}^{\mathrm{T}})]^{1/2}$ as a measure of the manipulability.

In the closed-loop pseudoinverse's method (CLP) the joint positions can be computed through the time integration of the velocities (12) according with the block diagram depicted in Fig. 2.

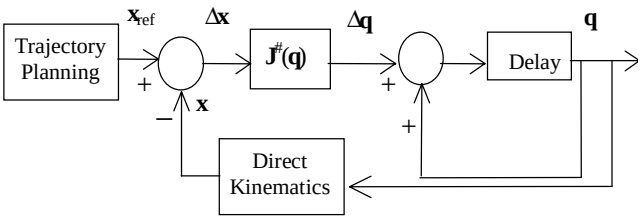

Fig. 2: Block diagram of the CLP algorithm.

An aspect revealed by the CLP is that repetitive trajectories in the operational space do not lead to periodic trajectories in the joint space [13-14]. This is an obstacle for the solution of many tasks because the resultant robot configurations have similarities with those of a chaotic system.

To overcome this problem other alternatives methods for trajectory planning were propose. For example the Open-Loop Manipulability (OLM) optimization method [14] gives superior results in what concerns a μ-optimization and the repeatability. Nevertheless, clear conclusions about the nature of the phenomena involved when using $\mathbf{J}^{\#}$ are still lacking.

In this paper we consider k-link planar manipulators. In this case, the direct kinematics and the Jacobian have simple recursive expressions:

$$\begin{bmatrix} x \\ y \end{bmatrix} = \begin{bmatrix} l_1C_1 + l_2C_{12} + l_3C_{123} + \cdots + l_kC_{12\ldots k} \\ l_1S_1 + l_2S_{12} + l_3S_{123} + \cdots + l_kS_{12\ldots k} \end{bmatrix} \tag{17}$$

$$\mathbf{J} = \begin{bmatrix} -l_1S_1 - \cdots - l_kS_{1\ldots k} & \cdots & -l_kS_{1\ldots k} \\ l_1C_1 + \cdots + l_kC_{1\ldots k} & \cdots & l_kC_{1\ldots k} \end{bmatrix} \tag{18}$$

where l_i is the length of link i, $S_{i\cdots k} = Sin(q_i + \cdots + q_k)$ and $C_{i\cdots k} = Cos(q_i + \cdots + q_k)$.

In this paper, during all the experiments, it is considered $\Delta t = 0.001$ sec $l_T = l_1 + l_2 + \ldots + l_k = 3$ m, $l_1 = l_2 = \ldots = l_k$, $m_T = m_1 + m_2 + \ldots + m_k = 3$ kg and $m_1 = \ldots = m$.

IV. CHAOS IN THE CLP CONTROL OF REDUNDANT MANIPULATORS

It is known that the CLP algorithm leads to unpredictable arm configurations, with responses similar to those of a chaotic system.

For example, Fig. 3 depicts the phase-plane joint trajectories for the 3*R*-robot positions, when repeating a circular motion with frequency $\omega_0 = 3$ *rad/sec*, centre at $r = [x^2+y^2]^{1/2} = 1$ and radius $\rho = 0.1$. Besides the position and velocity drifts, leading to different trajectory loops, we have points that are 'avoided'. Such points correspond to arm configurations where several links are aligned. This characteristic is inherent to the pseudoinverse matrix because the 3*R*-robot was tested both under open-loop and closed-loop control, leading to the same type of chaotic behaviour.

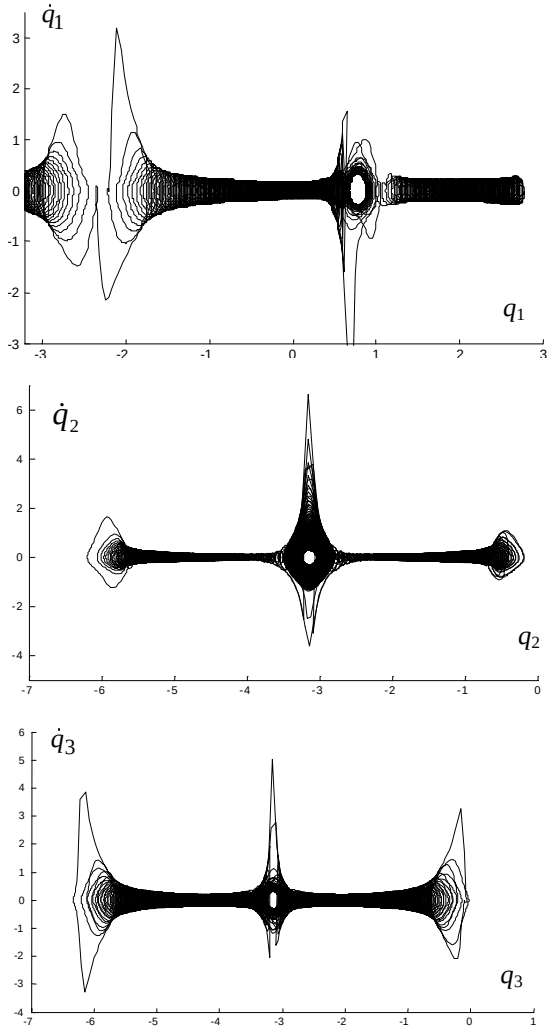

Fig. 3: Phase plane trajectory for the 3*R*- robot at $r = 1$, $\rho = 0.1$, $\omega_0 = 3$ *rad/sec*, $dim_C = 1.62$, $dim_L = 0.88$.

In order to gain further insight into the pseudoinverse nature, the robots under investigation were required to follow the cartesian repetitive circular motion for several radial distances r and radius ρ. The phase-plane joint trajectories were then analyzed and their fractal dimension estimated through the:

i) Lyapunov dimension

$$dim_L\ S = 1 - \frac{ln\,\lambda_1}{ln\,\lambda_2} \tag{19}$$

where λ_1 and λ_2 are the nonzero real eigenvalues of $\mathbf{J}\mathbf{J}^T$.
ii) Box-counting dimension

$$dim_C\ S = \lim_{\varepsilon \to 0} \frac{ln\,N(\varepsilon)}{ln\,(1/\varepsilon)} \tag{20}$$

where $N(\varepsilon)$ denotes the smallest number of bi-dimensional boxes of side length ε required in order to completely cover the plot surface S.

The CLP method leads to chaotic responses with fast transients and high accelerations. Applying expressions (18)-(19) to the results we get Fig. 4 revealing that:

- For the CLP method we have $dim_C > 1$ due to the position and velocity drifts, in contrast with the 'standard' case, that is, for non-redundant robot trajectories, where we have $dim_C = 1$.
- dim_C diminishes near the maximum radial distance $r = 3$.
- for each type of robot (*i.e.* 3*R* and 4*R*) dim_C is nearly the same, for all joints.
- As it is known from the chaos theory, in general $dim_L \neq dim_C$. Nevertheless, the locus $r = r_s$ ($r_s = 1$ and $r_s = 1.5$ for the 3*R* and 4*R* robots, respectively) seems to be, the limit between two distinct regions.
- For $r > r_s$ both the 3*R* and 4*R* robots have similar values both when using dim_L or dim_C

The chaos is due to the $\mathbf{J}^{\#}$ contribution to the manipulator inner motion. Nevertheless, a deeper insight into the nature of this motion must be envisaged. Therefore, several distinct experiments were devised in order to establish the texture of the Jacobian null space.

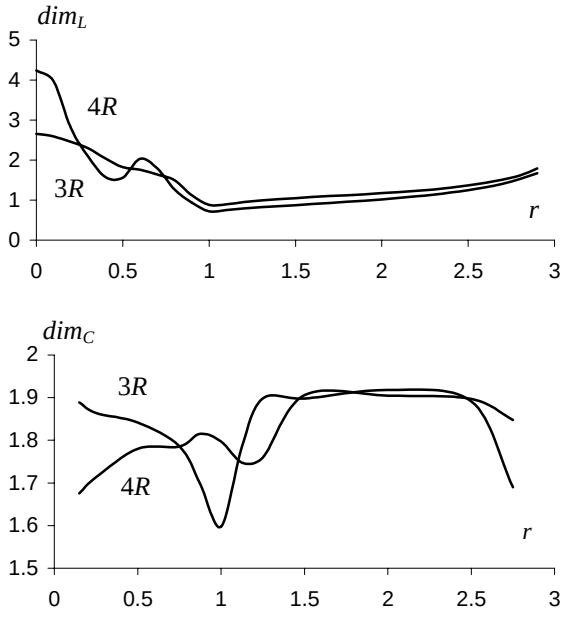

Fig. 4: Lyapunov (dim_L) and box-counting (dim_C) dimensions of the phase-plane *versus* r, for $\omega_0 = 3$ *rad/sec*, the 3*R* and 4*R* robots and $\rho = 0.1$.

In a first set of experiments the frequency response of the CLP method for the 3*R* and 4*R* robots is computed numerically for a doublet-like exciting signal at $0.9 < t < 1.1$ *sec* superimposed over the sinusoidal reference.

Figures 5-6 depict the 3*R* and 4*R* robot Bode diagrams for $r = 2$ and $\rho \in \{0.10, 0.25, 0.50, 0.75\}$. It is clear that the transfer matrix depends strongly on the amplitude of the 'exciting' signal ρ. Moreover, the Bode diagrams reveal that the CLP method presents distinct gains for the joint variables, according with the frequency, given by (i=1,…,n):

$$\left| q_i / x_{ref} \right| = k \left(s^{\alpha} + a \right) / \left(s^{\alpha} + b \right) \tag{21}$$

This conclusion is consistent with the phase-plane charts, that revealed low frequency drifts, while responding to an higher frequency (ω_0) input signal. Tables I-II show the values of the parameters of equation (21) and we see that $\alpha \approx 1$. For $|q_i / y_{ref}|$ we get the same conclusions.

The second set of experiments addresses also the frequency response, but in this case the exciting signal is distributed throughout the 500-cycle trajectories. Figures 7 and 8 depict the resulting amplitude Bode diagrams.

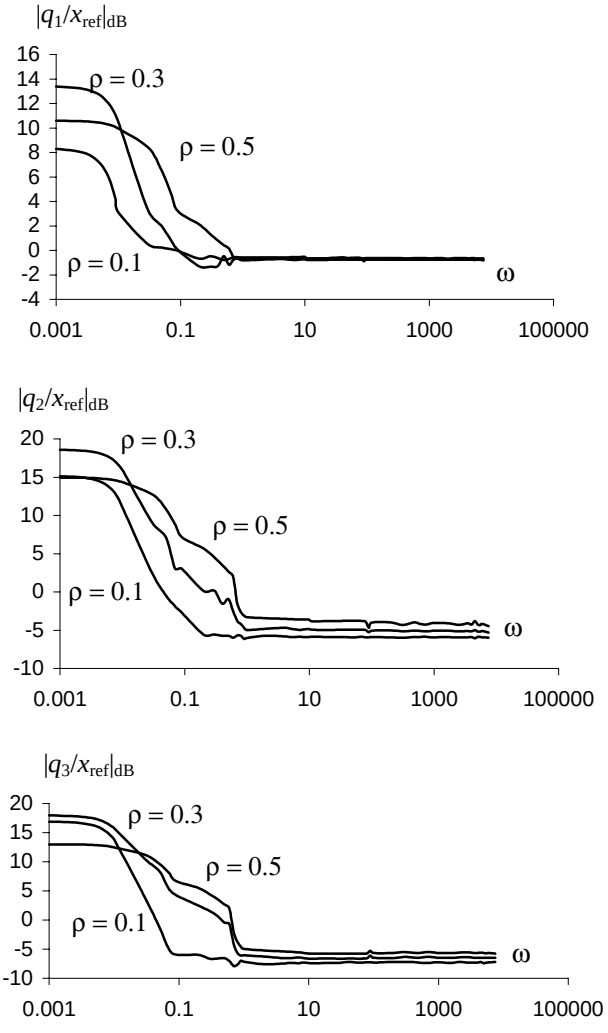

Fig. 5: Frequency response of the CLP method for the 3*R* robot $r = 2$, $\rho \in \{0.10, 0.30, 0.50\}$, $\omega_0 = 3$ *rad/sec*, with a doublet-like exciting signal

Table I
Bode diagrams parameters for 3*R* robot and a doublet-like exciting signal

	ρ	*a*	*b*	*k*	α
q_1/x_{ref}	0.10	0.01	0.004	0.96	1.09
	0.30	0.03	0.007	0.96	1.07
	0.50	0.18	0.050	0.95	0.89
q_2/x_{ref}	0.10	0.07	0.007	0.50	1.03
	0.30	0.31	0.02	0.55	0.88
	0.50	0.82	0.09	0.61	0.81
q_3/x_{ref}	0.10	0.06	0.004	0.44	1.14
	0.15	0.66	0.04	0.47	0.79
	0.50	0.86	0.10	0.52	0.87

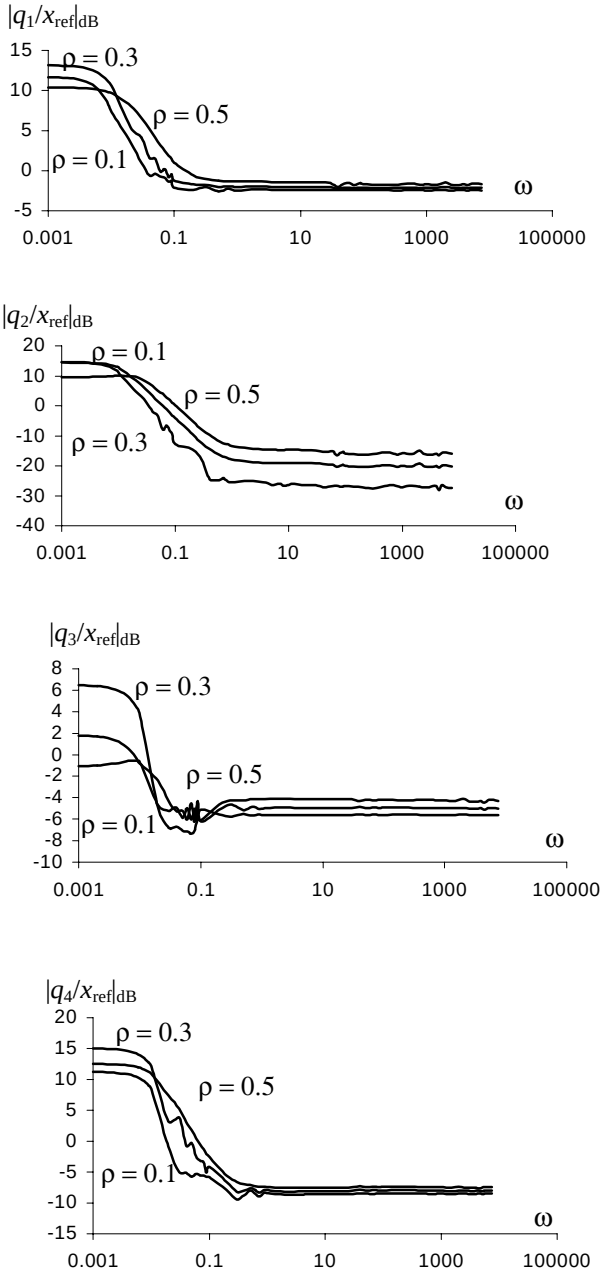

Fig. 6: Frequency response of the CLP method for the 4*R* robot, $r = 2$, $\rho \in \{0.10, 0.30, 0.50\}$, $\omega_0 = 3$ *rad/sec*, with a doublet-like exciting signal

Table II
Bode diagrams parameters for 4*R* robot and a doublet-like exciting signal

	ρ	*a*	*b*	*k*	α
q_1/x_{ref}	0.10	0.04	0.007	0.76	1.02
	0.30	0.05	0.009	0.78	1.02
	0.50	0.12	0.03	0.83	0.93
q_2/x_{ref}	0.10	0.61	0.005	0.04	1.06
	0.30	0.53	0.01	0.10	1.04
	0.50	0.73	0.04	0.16	0.98
q_3/x_{ref}	0.10	0.07	0.04	0.53	0.97
	0.30	0.01	0.006	0.56	1.09
	0.50	0.003	0.001	0.61	1.41
q_4/x_{ref}	0.10	0.04	0.004	0.38	1.12
	0.30	0.08	0.006	0.40	1.07
	0.50	0.20	0.02	0.42	0.91

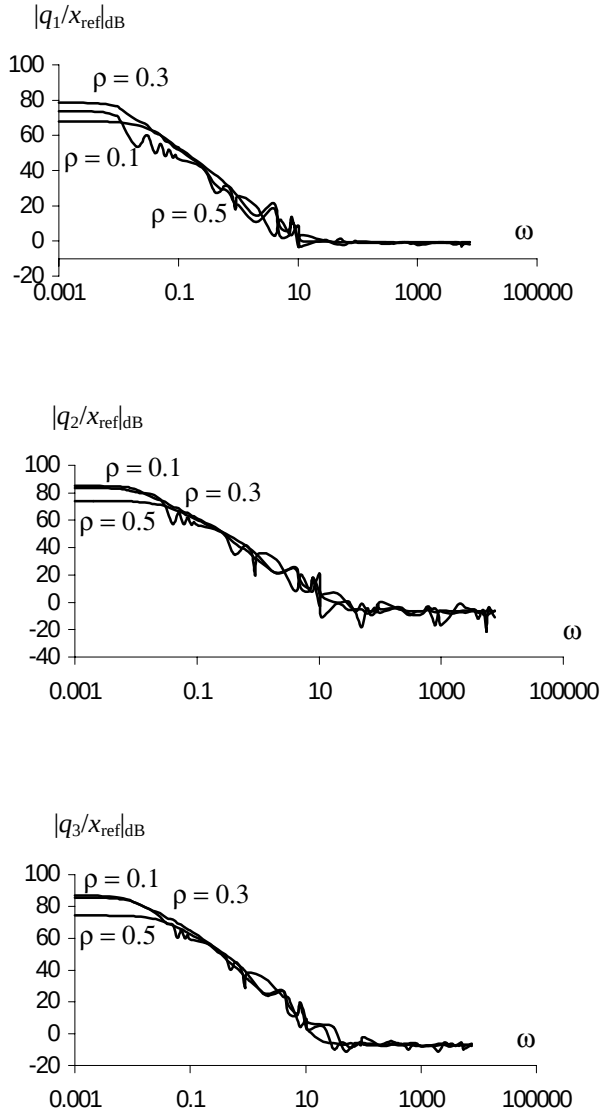

Fig. 7: Frequency response of the CLP method for the 3*R* robot, $r = 2$, $\rho \in \{0.10, 0.30, 0.50\}$, $\omega_0 = 3$ *rad/sec*, with white noise perturbation during all trajectory.

Table III

Bode diagrams parameters for the 3*R* robot and a white noise exciting signal distributed throughout the 500-cycle trajectories

	ρ	*a*	*b*	*k*	α
q_1/x_{ref}	0.10	15.8	0.003	0.93	1.13
	0.30	18.8	0.002	0.89	1.32
	0.50	30.3	0.01	0.83	1.23
q_2/x_{ref}	0.10	64.3	0.002	0.47	1.20
	0.30	82.9	0.002	0.43	1.34
	0.50	119.0	0.01	0.43	1.31
q_3/x_{ref}	0.10	101.0	0.002	0.43	1.26
	0.30	120.9	0.003	0.47	1.38
	0.50	130.0	0.01	0.40	1.33

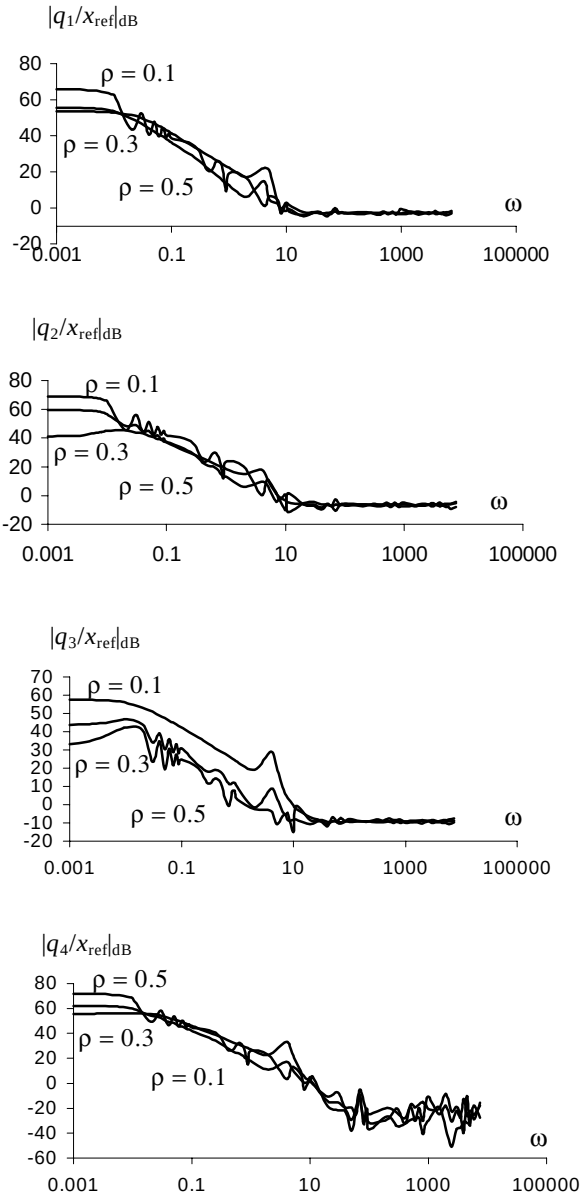

Fig. 8: Frequency response of the CLP method for the 4*R* robot, $r = 2$, $\rho \in \{0.10, 0.30, 0.50\}$ $\omega_0 = 3$ *rad/sec,* with white noise perturbation during all trajectory.

Table IV

Bode diagrams parameters for 4*R* robot, for exciting signal is distributed through out the 500-cycle trajectories

	ρ	*a*	*b*	*k*	α
q_1/x_{ref}	0.10	10.2	0.004	0.75	1.06
	0.30	7.7	0.01	0.77	1.02
	0.50	21.8	0.03	0.66	0.97
q_2/x_{ref}	0.10	139.9	0.003	0.8	1.15
	0.30	116.9	0.007	0.08	1.17
	0.50	263.2	0.03	0.07	1.20
q_3/x_{ref}	0.10	16.7	0.003	0.51	1.13
	0.30	10.6	0.006	0.55	1.08
	0.50	24.8	0.08	0.37	1.01
q_4/x_{ref}	0.10	2.7	0.02	0.36	1.05
	0.30	7.7	0.02	0.40	0.99
	0.50	47.2	0.02	0.31	1.00

In this case α takes fractional values (Tables III-IV), in contrast with the previous results. This is due to the memory-time property of *FDIs* because they capture the dynamic phenomena involved during all the time-history of the experiment. For y_{ref} we get the same conclusions.

In a third group of experiments, after elapsing a initial transient, we calculate the Fourier transform of the robot joint velocities for a large number of cycles of circular repetitive motion with frequency $\omega_0 = 3$ *rad/sec*.

Fig. 9-10 shows the results for the 3*R* and 4*R* robots versus the radial distance *r* the center of the circle with radius ρ = 0.1. Once more we verify that for $0 < r < r_s$ we get a signal energy distribution along all frequencies, while for $r_s < r < 3$ the major part of the signal energy is concentrated at the fundamental and multiple harmonics. Moreover, the DC component, responsible for the position drift, presents distinct values, according the radial distance *r* and ρ:

$$\left|\dot{q}_i(\omega = 0)\right| = a\rho^d / \left(b + r^c\right), \; i=1,2,\ldots,n. \qquad (22)$$

Table V show the values of the parameters of equation (22) for the 3*R* robot:

Table V

DC component parameters of Fourier transform for 3*R* robot joint velocities

	ρ	*a*	*b*	*c*	*d*
$\dot{q}_1(\omega = 0)$	0.005	480	0.16	3.40	2.10
	0.01	430	0.15	3.30	2.10
	0.05	235	0.16	4.80	1.90
	0.1	465	0.14	4.20	2.20
$\dot{q}_2(\omega = 0)$	0.005	315	0.96	3.20	1.90
	0.01	325	0.94	3.10	1.90
	0.05	385	1.43	3.10	1.90
	0.1	375	1.96	2.20	2.10
$\dot{q}_3(\omega = 0)$	0.005	250	0.73	1.70	1.90
	0.01	245	0.62	1.60	1.90
	0.05	320	1.30	1.90	1.90
	0.1	385	1.93	1.20	2.30

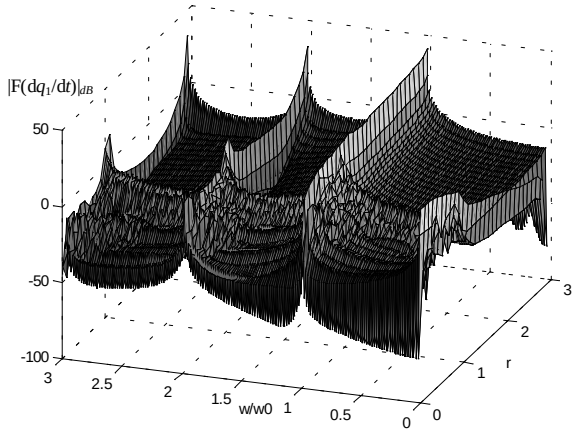

Fig. 9: Fourier transform of the 3*R* robot joint 1 velocity for 500 cycles, *vs r* and frequency ratio ω/ω_0, for $\rho = 0.1$, $\omega_0 = 3$ *rad/sec*

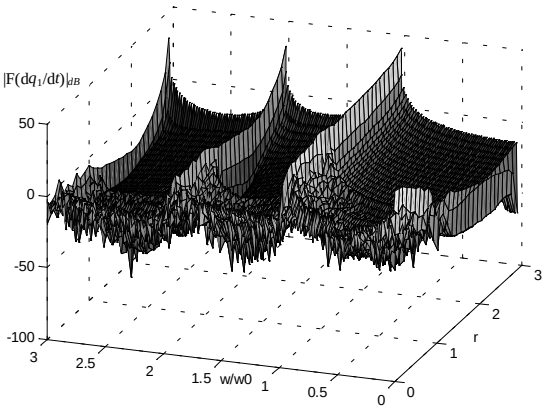

Fig. 10: Fourier transform of the 4*R* robot joint 1 velocity for 500 cycles, *vs r* and frequency ratio ω/ω_0, for $\rho = 0.1$, $\omega_0 = 3$ *rad/sec*

V. CONCLUSIONS

This paper discussed several aspects of the phenomena generated by the pseudoinverse-based trajectory control of redundant manipulators.

The CLP scheme leads to non-optimal responses, both for the manipulability and the repeatability. Bearing these facts in mind, the fractal dimension of the responses was analyzed showing that it is independent of the robot joint. In fact, the chaotic motion depends on the operational space point and on the amplitude of the exciting repetitive motion. In this perspective, the chaotic responses where analyzed from different point of views namely, phase-plane and frequency responses while considering a fractional calculus paradigm. The results are consistent and represent a step towards the development of superior trajectory planning algorithms for redundant and hyper-redundant manipulators.

REFERENCES

[1] J. A. Tenreiro Machado, "Analysis and Design of Fractional-Order Digital Control Systems", *SAMS* - Journal Systems Analysis-Modelling-Simulation, Gordon & Breach Science Publishers, vol. 27, pp. 107-122, 1997.

[2] J. A. Tenreiro Machado, "System Modeling and Control Through Fractional-Order Algorithms", *FCAA* - Journal of Fractional Calculus & Applied Analysis, vol. 4, n. 1, pp. 47-66, 2001.

[3] Andrew Gemant, On Fractional Differentials, *Philosophical Magazine*, vol. 25, pp. 540-549, 1938.

[4] Keith B. Oldham and Jerome Spanier, The Fractional Calculus: Theory and Application of Differentiation and Integration to Arbitrary Order, Academic Press, 1974.

[5] Bertram Ross (ed.), Fractional Calculus and Its Applications, *Lecture Notes in Mathematics 457*, Springer-Verlag, 1974.

[6] Stefan G. Samko and Bertram Ross, Integration and Differentiation to a Variable Fractional Order, *Integral Transforms and Special Functions*, vol. 1, no. 4, pp. 277-300, 1993.

[7] S. G. Samko, Fractional Integration and Differentiation of Variable Order, *Analysis Mathematica*, vol. 21, pp. 213-236, 1995.

[8] A. Oustaloup, La Commande CRONE: Commande Robuste d'Ordre Non Entier, Hermes, 1991.

[9] A. Oustaloup, B. Mathieu and P. Lanusse, The CRONE Control of Resonant Plants: Application to a Flexible Transmission, *European Journal of Control*, vol. 1, no. 2, pp. 113-121, 1995.

[10] Chiaverini, S, Singularity-Robust task-Priority Redundancy Resolution for Real Time Kinematic Control of Robot Manipulators. *IEEE Transactions Robotics Automation*, vol. 13, pp. 398-410, 1997.

[11] Conkur, E. S. and R. Buckingham, Clarifying the Definition of Redundancy as Used in Robotics. *Robotica*, vol. 15, pp. 583-586, 1997.

[12] Doty, K. L. and C. Melchiorri and C. Bonivento A Theory of Generalized Inverses Applied to Robotics. *Int, Journal of Robotics Research*, vol. 12, pp. 1-19, 1993.

[13] Duarte, F. B. and J. A T. Machado. Chaotic Phenomena and Performance Optimization in the Trajectory Control of Redundant Manipulators. *Recent Advances in Mechatronics*, Springer-Verlag, 1999.

[14] Duarte, F. B. and J. A. T. Machado, Chaos Dynamics in the trajectory Control of Redundant Manipulators. *IEEE International Conference on Robotics and Automation*, S. Francisco, USA, 2000.

[15] Theiler, J. Estimating Fractal Dimension. *Journal Optical Society of America*, vol. 7, nº6, pp. 1055-1073, 1990.

[16] Yoshikawa, T. Foundations of Robotics: Analysis and Control, MIT Press, 1988.